Subsurface microscopy of integrated circuits with angular spectrum and polarization control

F. H. Köklü,[1] S. B. Ippolito,[2] B. B. Goldberg,[1] and M. S. Ünlü[1,*]

[1]Department of Physics, Electrical and Computer Engineering and the Photonics Center, Boston University, 8 Saint Mary's Street, Boston, Massachusetts 02215, USA

[2]IBM Semiconductor Research and Development Center, Hopewell Junction, New York 12533, USA

*Corresponding author: selim@bu.edu

Received December 24, 2008; revised February 24, 2009; accepted March 11, 2009; posted March 16, 2009 (Doc. ID 105750); published April 10, 2009

We investigate the effect of an annular pupil-plane aperture in confocal imaging while using an NA increasing lens. We show that focal spot shape is highly sensitive to both polarization and angular spectrum of the incoming light. We demonstrate a lateral spatial resolution of 145 nm ($\lambda_0/9$) in the direction perpendicular to the polarization direction. © 2009 Optical Society of America

OCIS codes: 110.2945, 120.4630, 180.1790, 260.2110, 260.5430.

Development and implementation of optical methods for defect detection and imaging of silicon integrated circuits (ICs) have been crucial for the analysis and advancement of microelectronics [1–6]. Optical inspection through the backside of the silicon substrate is often necessary, because opaque interconnect metal layers hinder frontside optical microscopy. Optical analysis of ICs is accomplished by either excitation of circuit elements or collection of emission and scattering from the circuit at wavelengths greater than 1 μm, where the silicon substrate is relatively transparent. The restriction on the wavelength results in a limited lateral resolution of typically $\sim$1 μm in conventional microscopy. However, silicon IC fabrication technology, currently at the 45 nm process node and scaling down, requires an imaging resolution well beyond the capability of state-of-the-art conventional backside microscopy through the planar substrate surface [7]. Solid immersion microscopy techniques, in particular NA increasing lens (NAIL) microscopy demonstrated the ability of high-resolution backside imaging of silicon ICs [1]. A silicon NAIL placed on the backside of a silicon substrate effectively transforms the NAIL and the planar sample into an integrated solid immersion lens [8], increasing the NA by a factor of the square of the refractive index n to a maximum NA of 3.5, the refractive index of silicon. The impact of this immersion technique has been observed in wide field IC imaging [4] as well as point excitation and detection schemes [2,3].

Confocal laser scanning microscopes are commonly employed to simultaneously acquire electrical response and confocal reflection images. The spot size of the focused excitation beam determines the lateral spatial resolution of both methods. At high NAs, linearly polarized incoming light results in an elliptical focal spot [9] with significant differences in resolution in directions parallel and orthogonal to the polarization direction as observed recently in IC imaging using NAIL microscopy [6]. Annular pupil-plane apertures have been investigated and implemented to improve the resolution and functionality of various imaging systems [10–12]. Annular illumination modifies the focal field distributions, and this has been used to monitor the orientation of single molecules [12]. In this Letter, we mainly focus on the effect of annular apertures on the total focal spot shape. We experimentally demonstrate that tailoring the angular spectrum with an annular aperture while using linearly polarized illumination improves the spatial resolution in one direction significantly. Using a confocal microscope with a NAIL, we achieve a lateral spatial resolution of 145 nm ($\sim\lambda_0/9$) at $\lambda_0=1.3$ μm. Together with its contribution to longitudinal localization [5], angular spectrum tailoring proves to be a powerful and simple technique to improve the optical inspection of ICs.

The confocal microscopy setup is a single-path reflection-mode fiber-optical scanning microscope utilizing a single-mode fiber-coupled laser diode ($\lambda_0=1.3$ μm) and a 2×2 optical coupler instead of a beam splitter as shown in Fig. 1. For coupling in and out of the single-mode fiber, we use a collimating objective with matching NA, and a second objective with NA=0.26 is used for IC illumination and collection. A piezo stage forms an image by scanning the sample with the NAIL. The polarization direction of the incoming linearly polarized light is rotated by a

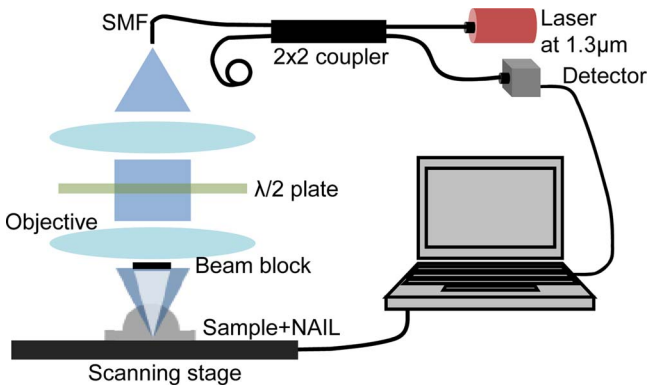

Fig. 1. (Color online) Experimental setup. Rotating the half-wave plate rotates the direction of polarization of the incoming light. By changing the height of the beam block we are able change the effective inner radius of the annular aperture. SMF, single-mode fiber.

half-wave plate located before the imaging objective. The angular spectrum is modified by blocking the center of the optical path in front of the imaging objective. The effective inner radius of the annular aperture can be changed by moving the beam block up and down.

The NAIL used in this Letter is an undoped silicon hemisphere with radius $R=1.61$ mm. The optimum substrate thickness (X) for aplanatic imaging with this NAIL is $X=R/n=460$ μm [13]. The sample is a custom IC with four metal and two polysilicon layers fabricated at Austriamicrosystems by a 0.35 μm process [4]. The substrate thickness was reduced to 458 ± 2 μm for aplanatic imaging. Imaging is performed on passive calibration structures that are embedded into the first polysilicon layer of the IC.

The goal of the first imaging experiment is to visually observe the effect of polarization and angular spectrum tailoring. A structure with four vertical and three horizontal lines with varying lengths is selected for this purpose. The linewidths and spacings are 0.35 μm. Figure 2 shows the images taken in two orthogonal polarization directions for three different pupil functions. In Fig. 2(a), we use a clear aperture. In Figs. 2(b) and 2(c), the circular beam block is located at the center of the optical path at increasing distances from the objective to provide different annular aperture geometries. The effective blocking radii are 1.7 and 3.5 mm, respectively, for the 6 mm radius back aperture. The arrows indicate the polarization direction. For each image pair, the sharpness of the horizontal and the vertical lines alternate owing to the orthogonal polarization directions used. In Figs. 2(b) and 2(c), the lines parallel to the polarization become sharper for annular aperture geometries. The signal coming from the lines perpendicular to the polarization weakens, since the overlap between the features and the elongated focal spot becomes smaller owing to annular illumination. This effect is accentuated in Fig. 2 for the annular aperture with a larger inner radius resulting in degradations in image quality. Furthermore, we observe ghost lines suggesting pronounced sidelobes.

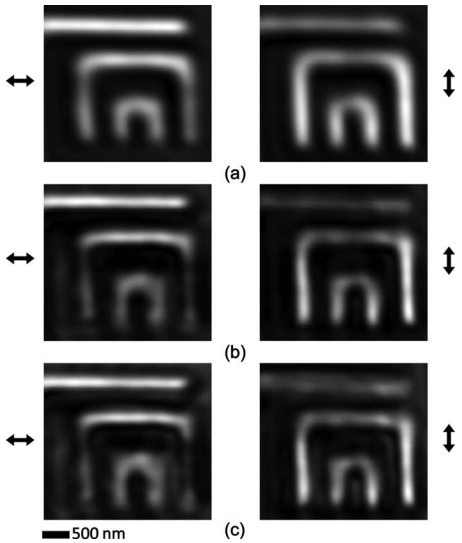

Fig. 2. Sample images taken on passive structures. (a) Images taken with a clear 6 mm radius back aperture for two polarization directions as indicated by the arrows. (b) Images taken using an annular aperture with an effective inner radius of 1.7 mm. (c) Same as (b) with an effective inner radius of 3.5 mm.

We used the Houston criterion to measure the resolution for different angular spectrum and polarization states. Edge responses were recorded at the edge of a 2-μm-wide line while rotating the polarization direction of the incoming linearly polarized light with 10° increments using a half-wave plate. Figures 3(a), 3(d), and 3(g) show the results for the corresponding pupil functions in Figs. 2(a)–2(c), respectively. Figures 3(b), 3(c), 3(e), 3(f), 3(h), and 3(i) show sample edge responses taken when the incoming light polarization is parallel and perpendicular to the edges, respectively, for each pupil function. The edge responses are fit to an error function, and the line spread functions (LSFs) are extracted. The spatial

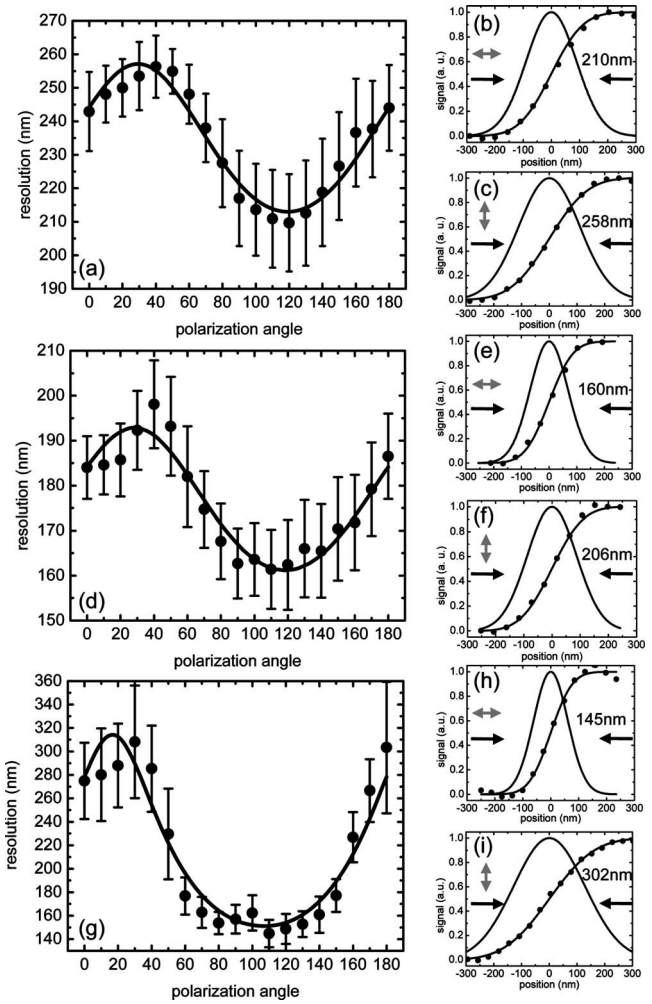

Fig. 3. Resolution measurements for different pupil functions. (a) Resolution is measured for a clear aperture while rotating the polarization direction from 0° to 180°. (b) Edge response data, error function fit, and LSF are shown for the horizontal polarization direction. (c) Same as (b) when the polarization direction is vertical. (d)–(f) Same as (a)–(c), respectively, when an annular aperture with an effective inner radius of 1.7 mm is used. (g)–(i) Same as (d)–(f), respectively, when the inner radius is 3.5 mm. Gray arrows indicate the polarization directions.

resolutions shown in Figs. 3(a), 3(d), and 3(g) are averaged over an edge of ~90 pixels to reduce the effect of local structural defects, and error bars show the standard deviation. The solid curve is the fit to these data, and the fitting function is the distance between two parallel tangent lines of an ellipse.

The measurements imply that the resolution changes in the range from 210 to 260 nm depending on the polarization direction for a clear aperture. For the annular aperture with a 1.7 mm inner radius, we observe a range of resolutions from 160 to 200 nm depending on the polarization direction. Finally, with the annular aperture having a 3.5 mm inner radius, we still see an improvement in one direction with a resolution of 145 nm, although the resolution in the other direction has degraded to a value of 300 nm.

We conducted theoretical calculations of the excitation and the detection point-spread functions (PSFs) of our imaging system using angular spectrum representation [9]. We extracted the LSFs of the whole system from the PSFs. Figure 4 depicts the LSFs for a linearly polarized excitation beam and a clear aperture in Fig. 4(a) and for annular apertures with effective inner radii of 1.7 mm and 3.5 mm in Figs. 4(b) and 4(c), respectively. The FWHMs for the calculated LSFs are 160 and 185 nm for the clear aperture, 150 and 177 nm for the first, and 127 and 195 nm for the second annular aperture. The relatively larger difference between the calculations and the measurements for the clear aperture case can be attributed to the relatively poor optical contact at the center of the NAIL-substrate interface. The results for the annular aperture are in good agreement with the calculations except the resolution in the polarization direction for the second annular aperture. The corresponding error could be due to low signal levels because of the large blocking radius, and this is evident from the large error bars in the measurements for this part. However, we can still observe the evolution of the FWHMs of the LSFs owing to angular spectrum tailoring. As illustrated in the calculations,

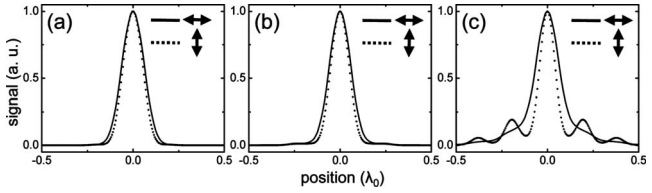

Fig. 4. (a)–(c) Calculated confocal LSFs for a clear aperture and two annular apertures with increasing inner radii, respectively. The arrows indicate the orthogonality.

for an annular aperture with a small inner radius, the FWHMs shrink in both directions. When the annular aperture has a larger inner radius, the FWHM continues to scale down in the perpendicular direction to the polarization, while sidelobes become more pronounced in agreement with the measurements. In the polarization direction, the FWHM starts to increase, which is also in agreement with the measurements except this is a slightly larger increase than expected.

We demonstrated a record lateral spatial resolution for one-photon excitation schemes by engineering the pupil function. We achieved a lateral spatial resolution of 145 nm ($\sim\lambda_0/9$) in the direction perpendicular to the polarization direction of the incoming light. Potentially a full high-resolution image can be constructed by acquiring additional images. Controlling the polarization and tailoring the angular spectrum in NAIL microscopy can significantly improve other optical analysis methods.

This work was supported by the Air Force Office of Scientific Research under grant MURI F-49620-03-1-0379.

References

1. S. B. Ippolito, B. B. Goldberg, and M. S. Ünlü, Appl. Phys. Lett. **78**, 4071 (2001).
2. S. B. Ippolito, S. A. Thorne, M. G. Eraslan, B. B. Goldberg, M. S. Ünlü, and Y. Leblebici, Appl. Phys. Lett. **84**, 4529 (2004).
3. E. Ramsay, K. A. Serrels, M. J. Thomson, A. J. Waddie, M. R. Taghizadeh, R. J. Warburton, and D. T. Reid, Appl. Phys. Lett. **90**, 131101 (2007).
4. F. H. Köklü, J. I. Quesnel, A. N. Vamivakas, S. B. Ippolito, B. B. Goldberg, and M. S. Ünlü, Opt. Express **16**, 9501 (2008).
5. S. B. Ippolito, P. Song, D. L. Miles, and J. D. Sylvestri, Appl. Phys. Lett. **92**, 101109 (2008).
6. K. A. Serrels, E. Ramsay, R. J. Warburton, and D. T. Reid, Nat. Photonics **2**, 311 (2008).
7. *International Technology Roadmap for Semiconductors* (2007).
8. S. M. Mansfield and G. S. Kino, Appl. Phys. Lett. **57**, 2615 (1990).
9. B. Richards and E. Wolf, Proc. R. Soc. London, Ser. A **253**, 358 (1959).
10. C. J. R. Sheppard and A. Choudhury, Appl. Opt. **43**, 4322 (2004).
11. G. M. Lerman and U. Levy, Opt. Express **16**, 4567 (2008).
12. B. Sick, B. Hecht, and L. Novotny, Phys. Rev. Lett. **85**, 4482 (2000).
13. S. B. Ippolito, B. B. Goldberg, and M. S. Ünlü, J. Appl. Phys. **97**, 053105 (2005).